EXPERIMENTS WITH A 2D OSCILLATING FOIL FOR PROPULSION AND MANEUVERING

F.S. Hover, D.A. Read, and M.S. Triantafyllou
Department of Ocean Engineering
Massachusetts Institute of Technology
Cambridge, MA 02139 USA

1 Abstract

Experiments were performed on an oscillating foil to assess its performance in producing large forces for propulsion and effective maneuvering. First, experiments on a harmonically heaving and pitching foil were performed to determine its propulsive efficiency under conditions of significant thrust production, as a function of the principal parameters: heave amplitude, Strouhal number, angle of attack, and phase angle between heave and pitch. Planform area thrust coefficients of 2.4 were recorded for 35 degrees maximum angle of attack and efficiencies of up to 71.5% were recorded for 15 degrees maximum angle of attack. A plateau of good efficiency, in the range of 50% to 60%, is noted. The introduction of higher harmonics in the heave motion, so as to ensure a sinusoidal variation in the angle of attack, produced a much higher thrust coefficient at high Strouhal numbers. Second, experiments on a harmonically oscillating foil with a superposed transient bias, as well as experiments on impulsively starting foils, were conducted to assess the capability of the foil to produce large lateral forces for maneuvering. Mean side force coefficients of up to 5.5 and instantaneous lift coefficients of up to 15 were recorded, demonstrating an outstanding capability for maneuvering force production.

2 Introduction

Fish, cetaceans, birds, and insects are, by engineering standards, astoundingly adept flyers and swimmers. The basic source of locomotion and maneuvering forces is the oscillating foil, which can generally undergo simultaneous translation and rotation in two or more degrees of freedom. The foils generate a large-scale vortex wake, which may appear in two distinct forms, one associated with drag and the other with thrust. The drag wake is analogous to the von Kármán street behind a bluff body, wherein the shed vortices induce a velocity in the opposite direction of the mean flow, resulting in a velocity deficit. Under proper conditions, a propulsive oscillating foil reverses the rotational direction in the wake structure so that the vortices induce a velocity in the same direction as the mean flow, creating a velocity excess, that is, a jet. In addition to efficient generation of propulsive force, (Hoppe, 1989, Triantafyllou *et al.*, 1993, Anderson *et al.*, 1998, Lighthill, 1969, Ellington *et al.*, 1996, Freymuth, 1988) unsteady vortex control creates very high lift coefficients for maneuvering (Gursul & Ho, 1992). An oscillating foil can further be used to manipulate incoming vorticity, and recapture vortical energy (Koochesfahani & Dimotakis, 1988, Cortelezzi *et al.*, 1997, Streitlien *et al.*, 1996, Gopalkrishnan *et al.*, 1994). With respect to applications, there has been recent work on underwater vehicle propulsion and maneuvering performed by, e.g., Bandyopadhyay *et al.* (1997) and Kato (1998). A more complete reference listing can be found in Triantafyllou & Yue (2000).

The present paper details a series of propulsion and maneuvering experiments performed with a heaving and pitching foil section, with measurement of lift and thrust forces, and pitching torque. First, we show systematic maps of efficiency and thrust coefficient, which indicate specific conditions of high performance under significant thrust production. Next, we performed tests on a flapping foil with a bias angle to measure the instantaneous and mean lift coefficient, which can generate the forces needed for maneuvering. Finally, we consider one-time impulsive maneuvers in still water, which are capable of generating extremely large instantaneous forces.

3 Experimental Methods

3.1 Apparatus

All experiments were conducted in the MIT Department of Ocean Engineering Testing Tank. The water tank itself is rectangular, with a working length of 18m, a 2.6m width, and a 1.4m depth. A mobile carriage, shown in Figure 1, contains the complete motion control and sensor system. A large servomotor positions the lower carriage through a linear bearing table, and a separate motor pitches the foil through a chain drive. Sensed variables include the vertical position of the foil (LVDT and heave motor encoder), angular position of the foil (potentiometer), pitch torque about the 1/3-chord

c	foil chord
s	foil span
U	steady towing speed
ρ	fluid density
ν	fluid kinematic viscosity
Re	chord Reynolds number, Uc/ν
α_{max}	maximum angle of attack
θ_0	amplitude of sinusoidal pitch $\theta(t)$
h_0	amplitude of nominally sinusoidal heave $h(t)$
A	wake width, approximated as $2h_0$
k	reduced frequency, $\omega c/2U$
St	Strouhal number, $2\pi\omega A/U$
$F_x(t)$	Thrust force; mean value $\overline{F}_x$
$F_y(t)$	Lift force; mean value $\overline{F}_y$
$P(t)$	Power supplied by actuators; mean value $\overline{P}$
C_T	mean thrust coefficient, $2\overline{F}_x/\rho U^2 cs$
C_L	mean lift coefficient, $2\overline{F}_y/\rho U^2 cs$
$C_{T_{SA}}$	mean thrust coefficient based on approximate swept area, $\overline{F}_x/\rho U^2 h_0 s$
$C_{L,max}$	maximum instantaneous lift coeff.
C_P	Power coefficient, $2\overline{P}/\rho U^3 cs$
η	Propulsive efficiency, $C_T U/C_P$

Table 1: Nomenclature.

pivot point, and forces exerted by the foil in the horizontal and vertical directions. We employed Kistler piezoelectric load cells for the torque and force measurements.

The foil used for all the experiments is rectangular with constant NACA 0012 section, chord 10 cm, and span 60 cm. It was constructed primarily of wood, with a fiberglass cloth and resin covering that provided an exceptionally smooth finish. Stainless steel axles were inserted on each end of the foil at the 1/3 chord position. Endplates were used on each strut to prevent flow around the ends of the foil and maintain approximately two-dimensional flow; the gap between plate and foil on each side was maintained at less than 2 mm.

Regular calibration verified consistently that all the sensors were linear to within 1.5% of the ranges encountered in the experiments. In addition to regular calibration, the pitch zero position was adjusted until the foil produced no lift. Finally, we performed tests to ensure that the extrapolation of force measurement at one end only was valid for loads applied across the span. The towing speed U was 0.40 m/s for all runs, corresponding to $Re = 4 \times 10^4$.

One of the most important parameters in this study is the Strouhal number based on heave amplitude:

$$St = \frac{4\pi h_0 \omega}{U} \tag{1}$$

where h_0 is the heave amplitude at the 1/3-chord point, and ω is the circular frequency in rad/s; the $2h_0$ term is an estimate of the width of the foil wake. Although the motion of the trailing edge is likely a better estimate of the wake width, for the purposes of these experiments with $\psi \approx 90°$, they are very close.

The average thrust force in propulsion tests is computed as follows:

$$\overline{F}_x = \frac{1}{T}\int_0^T F_x(t)dt, \text{ for } T >> 2\pi/\omega, \tag{2}$$

and the mechanical power delivered by the motors is given as

$$\overline{P} = \frac{1}{T}\left(\int_0^T F_y(t)\dot{h}(t)dt + \int_0^T Q(t)\dot{\theta}(t)dt\right). \tag{3}$$

See Table 1 and Figure 2 for nomenclature. In most cases presented U represents the towing velocity, but for impulsive-start experiments, where the carriage speed is zero, U represents the *maximum* heave velocity. Thrust and power coefficients may alternatively be defined by the swept area of the trailing edge instead of the planform area of the foil. As with the Strouhal number, this area can be approximated by just the product of span and double heave amplitude.

3.2 Foil Trajectory

Most of the propulsion experiments were conducted using sinusoidal motion for both the heave and pitch degrees of freedom. The heave and pitch motions are

$$h(t) = h_0 \sin(\omega t) \tag{4}$$
$$\theta(t) = \theta_0 \sin(\omega t + \psi). \tag{5}$$

so that ψ is the phase angle between pitch and heave in radians. The resulting angle of attack profile is related to the heave velocity and pitch angle:

$$\alpha(t) = -\arctan\left(\frac{\dot{h}(t)}{U}\right) - \theta(t) \tag{6}$$

The normal procedure is to fix U, ω, h_0 (thus defining the Strouhal number), phase angle ψ, and α_{max}. We then solve for the absolute pitch angle magnitude θ_0. An approximation for $\psi \simeq \pi/2$, and valid for low St, where the function $\arctan(x)$ is nearly linear in x, is

$$\theta_0 = \pi St + \alpha_{max}. \tag{7}$$

The phasing of α_{max} with regard to the harmonic motion in heave and pitch varies greatly over

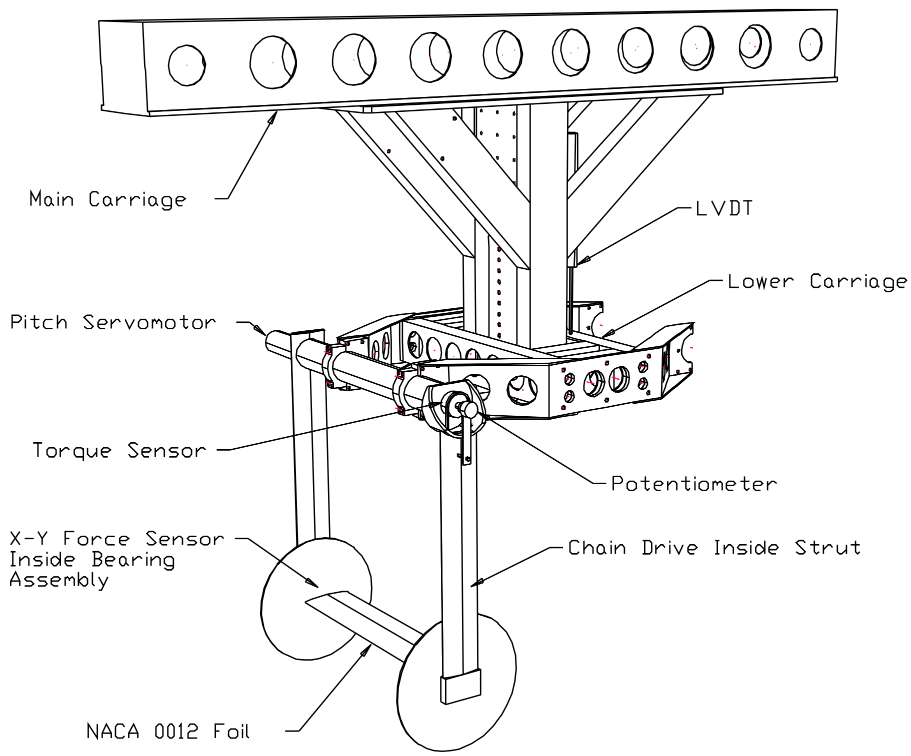

Figure 1: View of the test carriage, which oscillates the foil in heave and pitch.

this parametric set. In fact, the above equation has two solutions over a large range of frequencies, one corresponding to drag, and the other to thrust generation. This double solution in the angle of attack equation results from the fact that the foil can be pitched up or down with respect to the instantaneous oncoming flow. Figure 3 shows two θ_0 solutions, for the case $\alpha_{max} = 15°$ and several phase angles. The circled points are the terminal Strouhal numbers; the point where the thrust- and drag- producing values of θ_0 converge for each phase angle.

The angle of attack profile itself takes various forms, depending on the proximity of the θ_0 solution

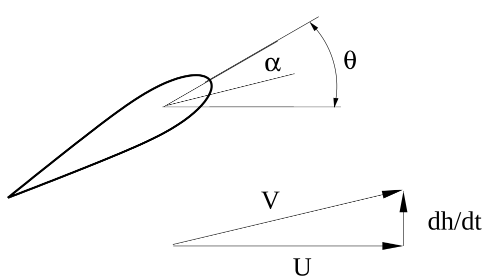

Figure 2: Foil parameters.

to the bifurcation point, i.e the terminal Strouhal number. For example, in Figure 4, the lowest value of St achieves nearly sinusoidal $\alpha(t)$, but as St increases, the α profile degrades sharply, through growing odd harmonics. In the case of $\psi \neq 90°$, the changes in $\alpha(t)$ evolve asymmetrically, but are otherwise similar.

The irregular angle of attack signal induced by high St could be eliminated through modifications to either or both the trajectory of $\theta(t)$ and $h(t)$. Without careful testing it would be difficult to assess clearly what combination of effects is best for recovering thrust. In this work, we consider a correction using heave alone, by expanding $\dot{h}$ using a power series, with the assumption of harmonic $\theta(t)$ and $\alpha(t)$. We then compute n (odd) superharmonic components in $\dot{h}$, which cancel out terms induced by the tangent function. This procedure can be streamlined so that one needs only to solve a well-posed n-dimensional linear system. The result is a set of coefficients to be implemented as:

$$\dot{h}(t)/U = H_1 \sin(\omega t) + H_3 \sin(3\omega t) + \cdots . \quad (8)$$

The effect of the third and fifth harmonics via this approach is shown in Figure 5; note that the graph shows $h(t)$ nondimensionalized with U and ω. The

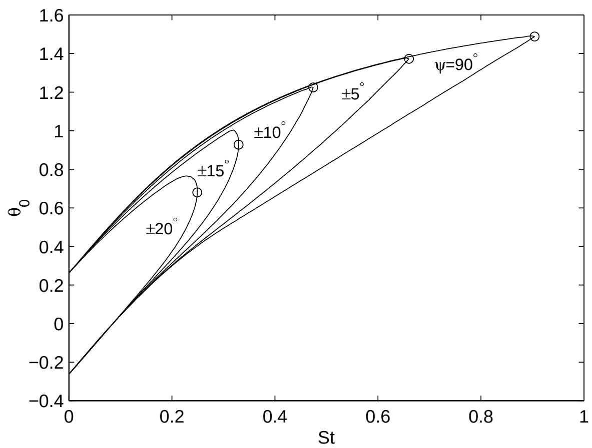

Figure 3: Bifurcation of the equation for maximum angle of attack α_{max}, showing both thrust- and drag-producing solutions for $\alpha_{max} = 15°$.

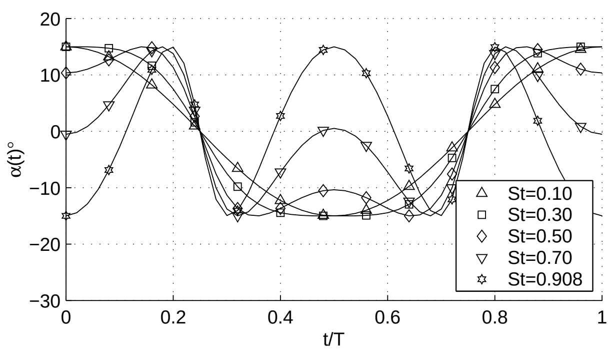

Figure 4: Angle of attack profile showing result of increasing Strouhal number for $\psi = 90°$, $\alpha_{max} = 15°$.

third and fifth harmonics change the baseline heave motion by less than six percent for the St range in this work, and so can be implemented easily; values are listed in Table 2. An alternative method for correction in the angle of attack has been given by Haugsdal (2000).

4 Propulsion Experiments

4.1 Simple Harmonic Motion

In Figures 6 and 7 we show the overall results of experiments conducted at $h_0/c = 0.75$ and 1.0, with 90° phase angle. Oscillations up to about 1.2 Hz were possible, giving a maximum Strouhal number of 0.44; α_{max} covers the range $[10 - 40]°$. Contours are calculated from experimental points taken at increments of 0.04 in St and 5° in α_{max}. At least two runs were conducted at each point to validate

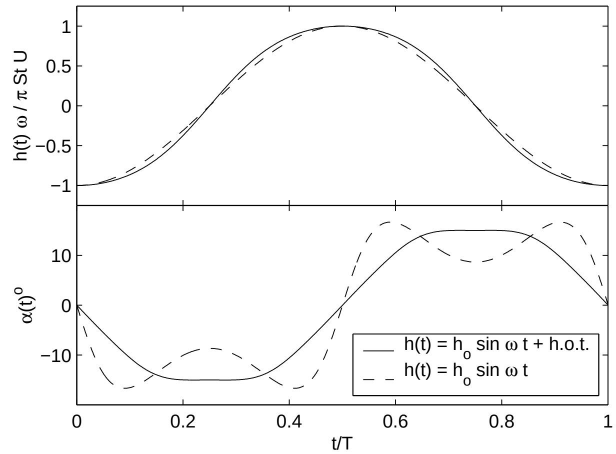

Figure 5: Effect of higher-order heave motion on angle of attack profile for $\psi = 90°, St = 0.60, \alpha_{max} = 15°$.

St	$H_1/\pi St$	$H_3/3\pi St$	$H_5/5\pi St$
0.20	1.010	-0.010	0.000
0.24	1.014	-0.015	0.000
0.28	1.019	-0.019	0.001
0.32	1.023	-0.024	0.001
0.36	1.028	-0.029	0.001
0.40	1.032	-0.034	0.002
0.44	1.036	-0.038	0.002
0.48	1.040	-0.043	0.002
0.52	1.044	-0.047	0.003
0.56	1.048	-0.051	0.003
0.60	1.051	-0.055	0.004

Table 2: Higher-harmonic components used for $\alpha_{max} = 15°$.

repeatability. As an aside, we also conducted experiments to determine the sensitivity to phase angle ψ. The results are reported elsewhere (Read, 1999), and it suffices for the present discussion to note that $\psi = 90°$ is generally the best choice; higher values may give small improvements in efficiency, but at the cost of reduced thrust.

First, we consider the case $h_0/c = 0.75$. C_T increases uniformly with St for high α_{max}, but at lower values of α_{max}, the available C_T levels off. At $\alpha_{max} = 10°$, for instance, the highest value is $C_T \approx 0.3$, achieved at the relatively low value $St = 0.32$. A maximum thrust coefficient of 1.10 exists around 30° α_{max} and $St = 0.44$ (the upper limit). At the other extreme, the zero contour of C_T represents the transition in the wake between drag- and thrust-producing vortex patterns. At low maximum angles of attack, this zero-crossing occurs at a low Strouhal number, around 0.06. As α_{max} increases,

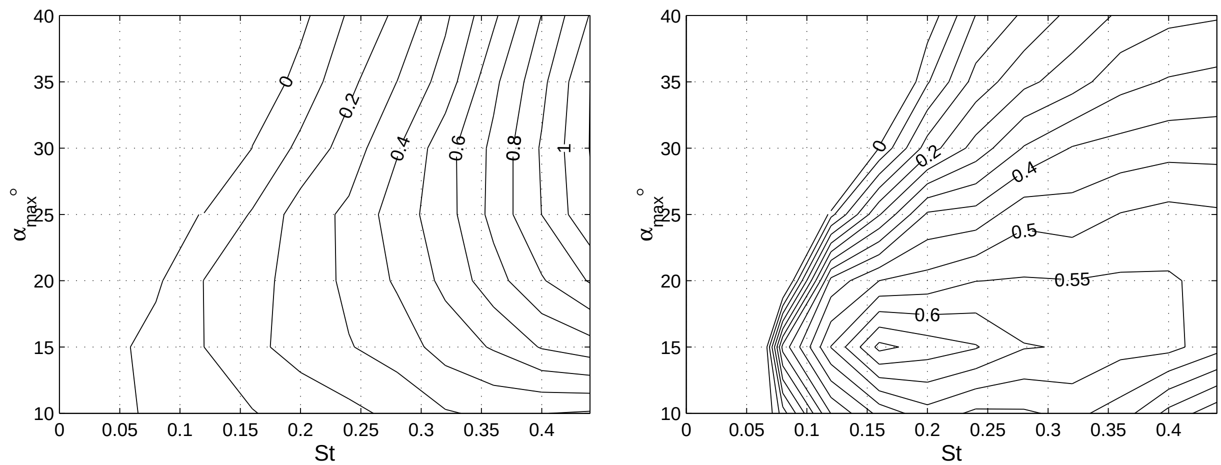

Figure 6: Contours of thrust coefficient (left) and efficiency (right) for $h_0/c = 0.75$ and $\psi = 90°$.

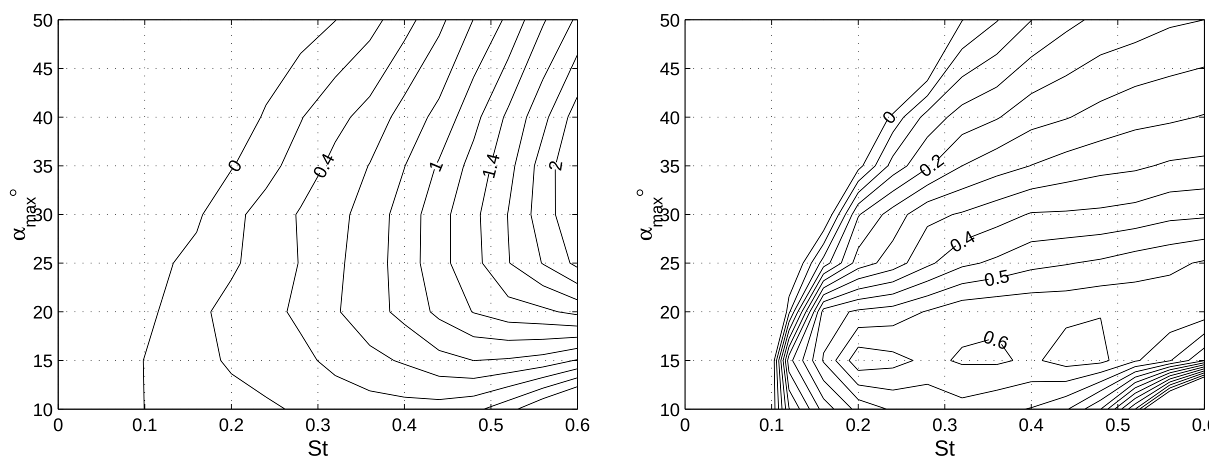

Figure 7: Contours of thrust coefficient (left) and efficiency (right) for $h_0/c = 1.00$ and $\psi = 90°$.

the transition occurs at higher and higher St.

A maximum propulsive efficiency of 71.5% was achieved at $\alpha_{max} = 15°$ and $St = 0.16$. This high efficiency peak is concurrent with a low thrust coefficient of only 0.18, however. Much more significant is the large 50%+ level of efficiency in the region of $St > 0.15$ and $\alpha_{max} = 15 - 25°$. In this regime, we find a run with 55.6% efficiency and $C_T = 0.79$, at $\alpha_{max} = 20°$ and $St = 0.40$. Similarly, at $\alpha_{max} = 25°$ and $St = 0.44$, we observe 50.8% efficiency and $C_T = 1.08$. These thrust coefficients correspond to swept-area thrust coefficients of $C_{T_{SA}} = 0.53$ and 0.72, respectively.

Figure 7 show the results of experiments conducted with a somewhat higher heave amplitude: $h_0/c = 1.00$, with $\psi = 90°$. Oscillations up to about 1.2 Hz were again possible, with the higher heave amplitude giving a maximum Strouhal number of 0.60. Maximum angle of attack varies from 10° to 50° for these tests.

The maximum thrust coefficient achieved is significantly higher than with $h_0/c = 0.75$, largely because of the larger Strouhal numbers which can be reached at the same dimensional frequency. For example, the highest C_T-value is 2.20 at $\alpha_{max} = 35°$ and $St = 0.60$. At the value $St = 0.44$, the limit of the $h_0/c = 0.75$ tests, we see $C_T \approx 1.15$ as a maximum value, achieved with $\alpha_{max} = 25 - 30°$; these results are close to those obtained with $h_o/c = 0.75$. Higher thrust is the product of larger motions, but efficiencies are slightly reduced, as might be expected from ideal propeller considerations. For instance, the highest C_T achieved with $h_0/c = 1.0$ corresponds with $\eta = 0.37$.

The peak efficiency of 63.4% ($St = 0.20$, $\alpha_{max} = 15°$), as before, correlates with a fairly low thrust coefficient of only 0.22. The efficiency contours show, however, that the $\eta = 50\%$ level extends all the way from $St = 0.15$ ($\alpha_{max} = 15 - 20°$), to $St = 0.60$ ($\alpha_{max} = 17 - 27°$). The high-St portion of this plateau corresponds with high thrust and efficiency: At $\alpha_{max} = 25°$ and $St = 0.60$, we find an efficiency of 55.6% and $C_T = 2.05$. This number translates to a swept area thrust coefficient of about $C_{T_{SA}} = 1.03$. These numbers reflect useful application to propulsion.

Again we note the zero-level contour of thrust coefficient. Trends are similar to those for the case $h_0/c = 0.75$, with the zero-crossing at lower Strouhal number for low α_{max} $(10 - 15°)$ and increasing for high angles of attack. With $h_0/c = 1.00$, however, the transition starts at $St = 0.10$ for low angles of attack and increases to about $St = 0.23$ for 40° angle of attack. At the highest angle of attack of 50°, which we did not test for $h_0/c = 0.75$, the transition occurs at a Strouhal number of over 0.32. Hence, drag can occur at values of St well within a high-efficiency operating range, if the angle of attack is too large.

Also of interest at $h_0/c = 1.0$ is the transition from thrust *back* to drag for high St and low α_{max}. We see this in Figure 7 for 10° angle of attack and $St \geq 0.54$. As discussed previously, lower angles of attack at high Strouhal number are more susceptible to multi-peaked angle of attack profiles. In this case, the angle of attack profile has become distorted enough to cause the foil to produce drag.

In general, some parametric combinations show promise for propulsion. Efficiency is quite high in some cases, but these peaks are not paired with good thrust performance. Large thrust coefficients are attainable with moderate to good efficiency, however. Both heave amplitudes show similar thrust performance, but lower mechanical frequencies allowed us to reach higher Strouhal numbers with the higher heave amplitude. On the other hand, the swept area thrust coefficients $C_{T_{SA}}$ are higher for the lower heave amplitude. Efficiency at low Strouhal number is better for $h_0/c = 0.75$, while efficiency at high Strouhal number (in the range of good thrust performance) appears slightly better for $h_0/c = 1.00$.

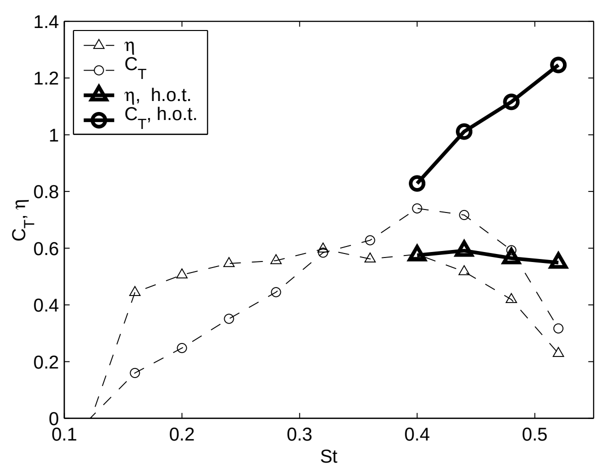

Figure 8: Effect of higher-order heave motion for $\alpha_{max} = 20°$, $\psi = 100°$, $h_0/c = 1.00$.

α_{max}	ψ	St	C_T	C'_T	η	η'
15°	80°	0.32	0.30	0.32	0.61	0.56
		0.36	0.25	0.37	0.52	0.57
		0.40	0.16	0.43	0.40	0.60
	90°	0.48	0.80	0.82	0.61	0.58
		0.52	0.78	0.95	0.56	0.59
		0.56	0.72	1.06	0.50	0.56
		0.60	0.58	1.21	0.41	0.56
	100°	0.32	0.33	0.41	0.52	0.58
		0.36	0.31	0.44	0.45	0.52
		0.40	0.18	0.54	0.25	0.51
20°	80°	0.40	0.60	0.69	0.63	0.61
		0.44	0.51	0.77	0.57	0.60
		0.48	0.41	0.88	0.52	0.61
		0.52	0.18	0.90	0.40	0.57
	90°	0.48	1.21	1.11	0.60	0.59
		0.52	1.31	1.31	0.59	0.60
		0.56	1.39	1.52	0.58	0.59
		0.60	1.45	1.71	0.58	0.58
	100°	0.40	0.74	0.83	0.58	0.58
		0.44	0.72	1.01	0.52	0.59
		0.48	0.59	1.12	0.42	0.57
		0.52	0.32	1.25	0.23	0.55
25°	80°	0.52	1.04	1.38	0.58	0.57
		0.56	0.97	1.52	0.58	0.56
		0.60	0.79	1.73	0.54	0.57
	100°	0.52	1.33	1.61	0.54	0.54
		0.56	1.29	1.89	0.51	0.55
		0.60	1.11	2.09	0.44	0.53
30°	100°	0.52	1.77	1.78	0.50	0.49
		0.56	1.96	2.06	0.51	0.48
		0.60	2.15	2.43	0.52	0.49

Table 3: Effects of higher-order heave motion to eliminate distortion in angle of attack. C_T and η values for the nominal case of sinusoidal heave motion are from the contours of Figure 7.

4.2 Higher-Order Heave Motion

As noted above, small efficiency increases are seen for phase angles other than the nominal value of 90°. However, if these efficiency increases occur at high St (i.e. close to the terminal value), they are generally accompanied by declining thrust performance associated with distorted angle of attack profiles. More frequently, however, phase angles other than 90° showed worse efficiency at high Strouhal number, mimicking the decline in thrust performance. In an effort to recover this lost performance, foil kinematics were altered in such a way that the angle of attack profile retained a generally sinusoidal shape, avoiding forms with more than two peaks per cycle. Namely, the heave motion was changed to include third and fifth order terms, as described in Section 3; the results of the experiments conducted with this higher-order heave motion are given in Table 3. All experiments of this type were conducted at $h_0/c = 1.00$.

As an example case, Figure 8 indicates that the effect of the higher-order heave motion is a continuation of the nominal C_T vs. St line, which normally degrades with the angle of attack at high St. Efficiency is also sustained at a plateau by the higher-order motion, whereas with sinusoidal heave motion, it typically falls off to very poor levels at high St.

At $\psi = 90°$ there is significant improvement in efficiency due to the higher-order heave motion for $\alpha_{max} = 15°$, but a smaller effect at $\alpha_{max} = 20°$. This characteristic can be predicted from the contour plots of Section 4.1, in which the high-efficiency plateau extends to $St = 0.60$ for $\alpha_{max} = 19 - 27°$.

For $\alpha_{max} = 25°$, higher-order heave motion experiments were conducted at $\psi = [80, 100]°$. The trends are the same as at lower α_{max}, but very high values of C_T are now possible. For $\psi = 80°$ and $St = 0.60$, for instance, efficiency increases slightly from 54% to 57%, and thrust coefficient improves from 0.79 to 1.73. For $\psi = 100°$, efficiency at $St = 0.60$ increases from 44% to 53%. The thrust coefficient here improves from 1.11 to 2.09.

The higher-order heave motion experiments are quite encouraging. Small changes in the heave motion can effect drastic changes in performance by preventing corrupted angle of attack profiles. Since the distorted angle of attack profile is no longer present, the performance decline caused by phase angles other than 90° is largely negated. The highest thrust coefficient recorded in this work occurred during one of these experiments ($C_T = 2.43$ for $\psi = 100°$, $\alpha_{max} = 30°$). These results suggest that controlling the angle of attack through slight modifications to foil motion should be studied further.

5 Maneuvering

5.1 Pitch Bias

During straight-line, symmetric propulsion, an oscillating foil device produces instantaneous force vectors with relatively small thrust components. Most of the force produced by the foil is in the form of lift; symmetry causes the mean lift to be zero. By adding a bias, or static offset, to the angle of attack, one can take advantage of these large lift forces for maneuvering. The simplest method is to add bias to the pitch angle itself, which is linearly related to the angle of attack.

Experiments were conducted in the parameter space of good thrust-production in propulsion: $\psi = 90°$, $\alpha_{max} = [25, 30, 35]°$. A phase angle of 100° was also tested at $\alpha_{max} = [30, 35]°$ since these runs produced very high thrust in straight propulsion. All pitch biases were positive to direct flow away from the free surface; the heave motion was $h_0/c = 1.00$. For each set of parameters, the mean lift and thrust coefficient over one cycle are given. Since these forces would be transient in a real application, the maximum instantaneous lift coefficient is also recorded.

Example time traces in Figure 9, for bias angles of 10° and 60°, verify the desired effect. With a small bias angle, the vertical force possesses an asymmetry with both positive and negative regions. The thrust force varies at twice the frequency as expected, and has short periods of negative (drag) force. Larger bias angles create vertical forces which are of one sign only, and characterized by strong peaks. The concurrent horizontal force is entirely in the drag direction.

The mean lift and thrust coefficients are given in Figure 10, wherein the horizontal axis represents C_T and the vertical axis C_L. Each curve covers a range of bias angles; the zero bias angle always provides near zero mean lift. Adding a pitch bias always decreases the thrust coefficient, although small bias angles still produce useful amounts of thrust. Finally, the effects of high St seem to diminish in the drag regime; above 30° bias angle, the thrust coefficient appears to be almost independent of St. The data for $St = 0.60$ are summarized in Table 4.

We are merging our control surface and propulsor into one device, so that comparing the forces reported here to, say, the lift to drag (L/D) ratio of a wing or rudder is difficult. The magnitude of both drag and thrust achieved here are generally much larger than the steady drag of a streamlined wing, leading to low ratios of L/D relative to these wings. On the other hand, we can also produce a pure lift force. In this case the drag would approach zero and L/D would approach infinity. In any event, the values of mean lift are large relative to a steady flow case. For the case of a 30° bias, the angle of attack over one cycle will have a minimum of 0° and maximum of 60° (when non-biased maximum angle of attack is 30°). The stall angle for a NACA 0012 foil is approximately 16°, so stall is likely taking place over part of each cycle. A rudder of this equivalent section would have a steady maximum lift coefficient of about 1.6, at 16° angle of attack, just before stall. The very large values of mean lift coefficients we have observed could only be obtained in steady flow using multiple slat and flap wings or boundary layer control.

ψ	α_{max}	C_T	C_L	$max(C_L)$
90°	25°	-0.82	4.7	11.9
†90°	25°	-3.04	5.5	16.6
90°	30°	-0.55	4.2	12.7
90°	35°	-0.70	4.4	13.5
100°	30°	-0.94	4.9	13.3
100°	35°	-0.61	4.5	13.8

†: bias angle 60°

Table 4: Force coefficients for 30° pitch bias, $St = 0.60$.

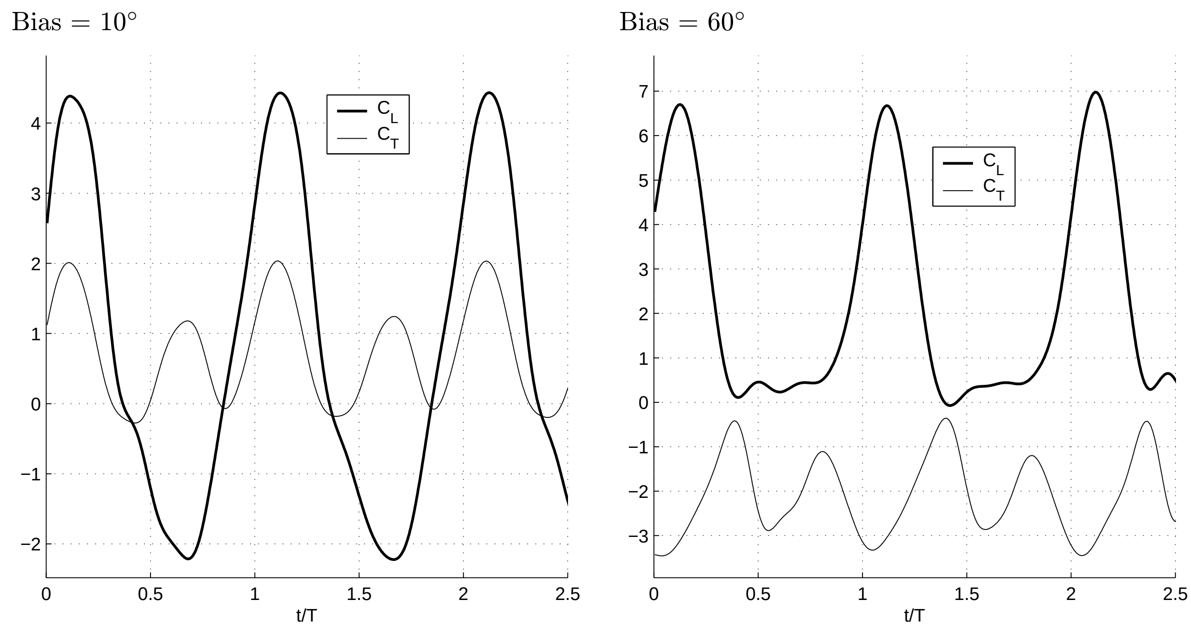

Figure 9: Lift and thrust coefficient traces during bias tests, $\psi = 90°$, $\alpha_{max} = 25°$, $St = 0.40$.

ψ	α_{max}	C_L	bias
90°	25°	3.94	24.3°
90°	30°	4.07	25.4°
90°	35°	3.93	24.5°
100°	30°	4.34	24.0°
100°	35°	4.29	24.1°

Table 5: Estimated pure lift coefficients and bias angles for zero thrust, $St = 0.60$.

Comparing the estimated mean lift coefficients achieved at zero thrust level (Table 5), we note that 100° phase angle shows slightly more mean lift. We also note that 30° maximum angle of attack (with respect to zero bias angle) shows the highest performance in both the 90° and 100°phase angle cases. The bias angles resulting in zero thrust force are quite close together (near 24.5°), even though there is a 10° difference in α_{max}.

Pitch bias is a simple and effective way to obtain maneuvering forces from a foil propulsion system, through unsteady effects. Very large drag forces can also be generated, exceeding those of the symmetric braking solution; see Read (2000).

5.2 Impulsive Starting

A related problem in maneuvering involves forces created when the foil moves through a single sweep, in still water. A smooth trajectory is illustrated in Figure 11, where the trailing edge sweeps out an arc as the heave and pitch go through half-sinusoidal trajectories, with finite acceleration. We performed tests also with other trajectories, but found ringing in the force signals whenever the velocity was discontinuous. The force response (Figure 12) is typified by a single large peak in lift force, and two smaller peaks in thrust, which are obviated by a long drag period following. In the data shown, the drag period occurs after the motion is complete.

$\dot{h}(max)$	C_T(max)	C_L(max)
0.50	5.4	7.9
0.57	5.5	8.3
0.63	5.1	7.7
0.69	5.3	8.1
0.75	5.3	8.0

Table 6: Instantaneous thrust and lift coefficients during a one-time starting maneuver.

Nondimensionalization of the forces is performed using the usual lift and drag coefficients, but with the maximum heave velocity. Instantaneous thrust and lift values scale closely with this reference velocity squared, causing the coefficients to take roughly constant values; see Table 6. Since the motions are harmonic, the forces can be correlated directly with acceleration, and hence with added mass. Consequently, no upper limit exists for the fluid forces which can be generated; rather, the constraint is the force which can be sustained by the device.

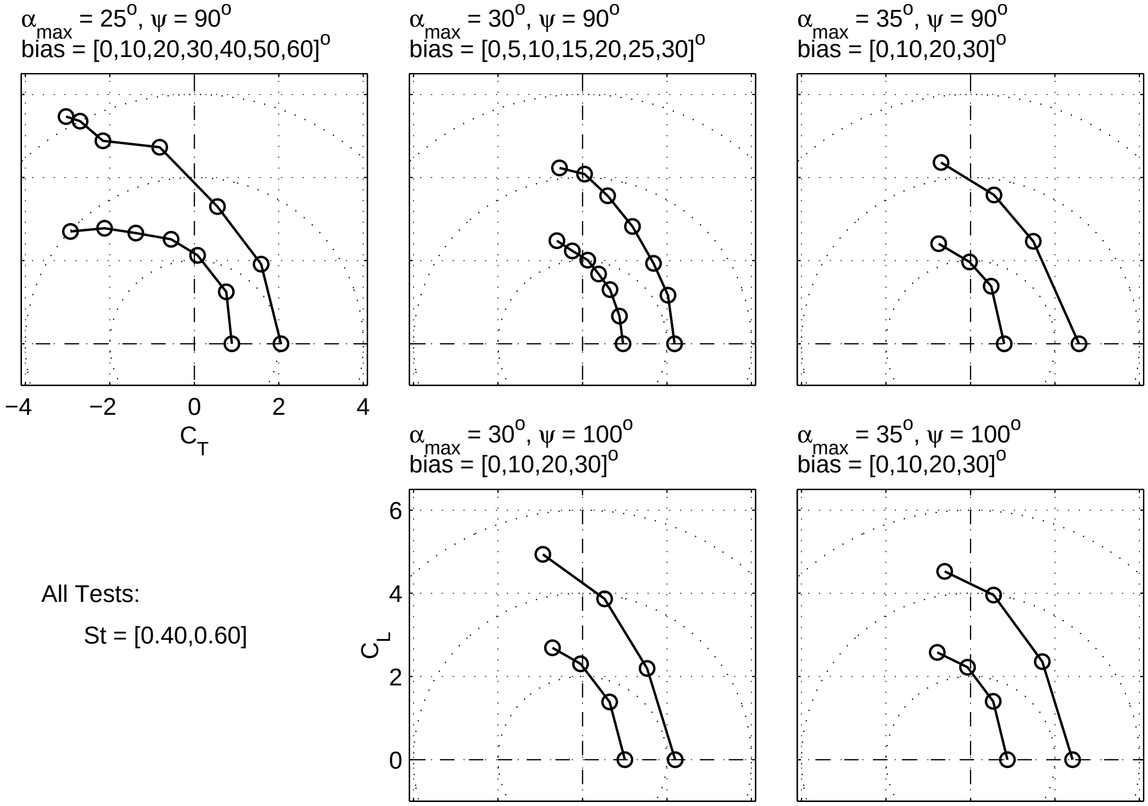

Figure 10: Mean C_T and C_L points for tests with pitch bias.

6 Discussion and Summary

Under the proper conditions, the propulsive performance of an oscillating foil is good. The highest propulsive efficiency we achieved was 71.5%, with a corresponding thrust coefficient of 0.18, in line with the generally good efficiency of lightly-loaded propulsors. Conversely, a thrust coefficient of 2.43 occurred during one experiment with higher-order heave motions, with $\alpha_{max} = 30°$, $\psi = 100°$, and $St = 0.60$; the efficiency was 49%. Besides these maxima, we can also note broad efficiency plateaus in both the $h_0/c = 0.75$ and $h_0/c = 1.00$ cases. These plateaus represent large areas of the parameter space in which routine efficiencies greater than 50% can be achieved. There are also conditions for which higher C_T could be expected, if St can be increased beyond the limits of our experiment. In particular, the higher-order heave correction may extend the high-efficiency plateau significantly (Haugsdal, 2000).

Maneuvering tests with the oscillating foil are perhaps more promising, especially with regard to existing control surfaces operating in steady flow. By adding pitch bias to the harmonic motion, large lift coefficients can be achieved; the largest mean and instantaneous values are $C_L = 5.5$ and 16.6, respectively. These values were achieved for Strouhal number 0.60, the maximum level we could achieve with our apparatus. Therefore it seems likely that even larger values would be possible for higher St. Large lift values are generally accompanied by a large drag force, representing a braking force in the context of a marine vehicle. For certain values of α_{max} near 25°, referenced to zero-bias case, zero drag can be achieved. In general, the total force vectors for pitch bias cases are always larger than those of propulsion cases.

The lift coefficient due to a bias increases with Strouhal number, the highest values always occurring at the highest tested Strouhal number of 0.60, or a reduced frequency of $k = 0.94$. In comparison, the oscillating flow experiments of Gursul & Ho (1992) indicated an optimum value of about $k = 0.80$, where their lift coefficients showed a maxima. Another estimate for the optimum k, based on vortex wavelength, is $k \approx 1$. Hence, it is possible that our Strouhal number limit is near an optimum value, and that the lift coefficient would begin to decrease if higher Strouhal numbers could be tested.

ACKNOWLEDGEMENTS: Support from the Office of Naval Research, under contract number N00014-99-1-1082 and monitored by Dr. Teresa McMullen, and the MIT Sea Grant Office under contract number NA86RG0074, is gratefully acknowledged. D.R. was also supported by the MTS Systems Corporation George Butzow Fellowship.

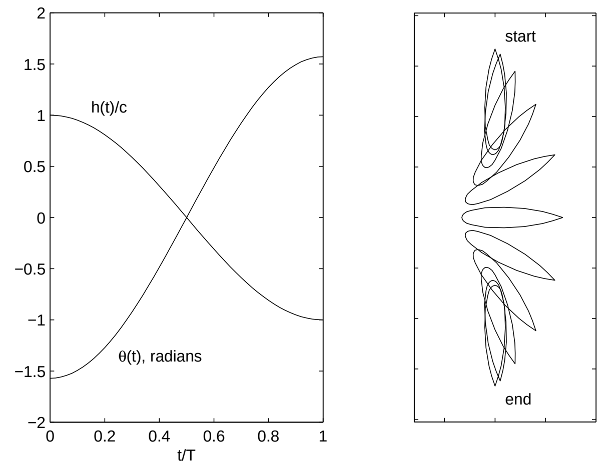

Figure 11: Foil trajectory for impulsive starting maneuver.

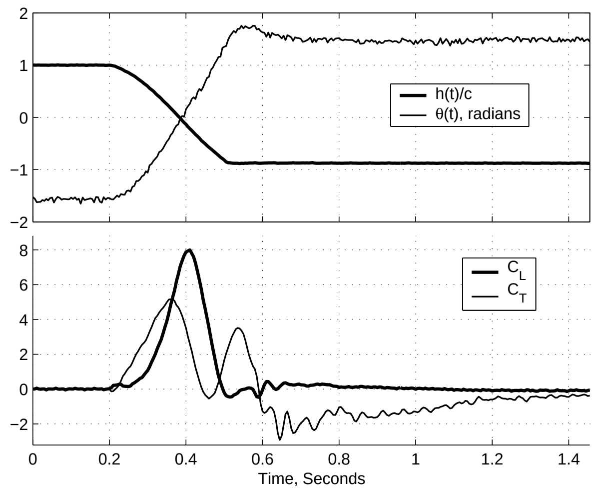

Figure 12: Results of an impulsive starting maneuver, with maximum heave velocity $0.754 m/s$. *Top*: heave and pitch motion, *bottom*: lift and thrust coefficients.

REFERENCES

ANDERSON, J.M., K. STREITLIEN, K., BARRETT, D.S., & TRIANTAFYLLOU, M.S. 1998 Flapping foils of high propulsive efficiency. *J. Fluid Mech.* **360**, 41-72.

BANDYOPADHYAY, P., CASTANO, J., RICE, J., PHILLIPS, R., NEDDERMAN, W., & MACY, W. 1997 Low-speed maneuvering hydrodynamics of fish and small underwater vehicles. *J. Fluids Eng.* **119**, 136-44.

CORTELEZZI, L., CHEN, Y.-C., & CHANG, H.-L. 1997 Nonlinear feedback control of the wake past a plate: from a low-order model to a higher-order model. *Phys. Fluids* **9**, 2009-22.

ELLINGTON, C.P., VAN DEN BERG, C., & THOMAS, A. 1996 Leading edge vortices in insect flight. *Nature* **384**, 6-26.

FREYMUTH, P. 1988 Propulsive vortical signature of plunging and pitching airfoils. *AIAA J.*, **26**, 881-3.

GOPALKRISHNAN, R. and TRIANTAFYLLOU, M.S., TRIANTAFYLLOU, G.S., & BARRETT, D.S. 1994 Active vorticity control in a shear flow using a flapping foil. *J. Fluid Mech.* **274**, 1-21.

GURSUL, I. & HO, C.M. 1992 High aerodynamic loads on an airfoil submerged in an unsteady stream. *AIAA J.* **30**, 1117-9.

HAUGSDAL, Ø. 2000 Motion control of oscillating foils for steady propulsion and starting maneuvers. SivilIngeniør Thesis, Norwegian University of Science and Technology.

HOPPE, K.G. 1989 The dynamo-elastic oscillating foil propeller. *Schiff Hafen* **5**, 54-61.

KATO, N. 1998 Locomotion by mechanical pectoral fins. *J. Mar. Sci. Tech.* **3**, 113-21.

KOOCHESFAHANI, M.M., & DIMOTAKIS, P. 1988 A cancellation experiment in a forced turbulent shear layer. *AIAA Tech. Paper* 88-3713-CP.

LIGHTHILL, M.J. 1969 Hydromechanics of aquatic animal propulsion. *Ann. Rev. Fluid Mech.* **1**, 413-45.

READ, D.A. 2000 Oscillating foils for propulsion and maneuvering of ships and underwater vehicles. M.S. Thesis, Massachusetts Institute of Technology.

STREITLIEN, K., TRIANTAFYLLOU, G.S., & TRIANTAFYLLOU, M.S. 1996 Efficient foil propulsion through vortex control. *AIAA J.* **34**, 2315-19.

TRIANTAFYLLOU, G.S., TRIANTAFYLLOU, M.S., & GROSENBAUGH, M.A. 1993 Optimal thrust development in oscillating foils with application to fish propulsion. *J. Fluids Struct.*, **7**, 205-24.

TRIANTAFYLLOU, M.S., TRIANTAFYLLOU, G.S., & YUE, D. K.-P. 2000 Hydrodynamics of fishlike swimming. *Ann. Rev. Fluid Mech.*, **32**, 33-53.